Reassessing long-term exhumation rates in magmatic terranes

F.J. Cooper[a,b], B.A. Adams[a,b], S.I.R. Dahlström[b], T.A. Ehlers[c,d], M.C. van Soest[e], K.V. Hodges[e], B.R. Jicha[f], B.S. Singer[f], J. Cortes Yañez[g,1], R.J. Perkins[h]

[a]Department of Earth Sciences, University College London, London, UK.
[b]School of Earth Sciences, University of Bristol, Bristol, UK.
[c]Department of Geosciences, University of Tübingen, Tübingen 72074, Germany.
[d]School of Geographical and Earth Sciences, University of Glasgow, Glasgow, UK.
[e]School of Earth and Space Exploration, Arizona State University, Tempe, Arizona, USA.
[f]Department of Geoscience, University of Wisconsin-Madison, Madison, Wisconsin, USA.
[g]BHP Copper Exploration, Las Condes, Santiago 7560623, Chile
[h]BHP, 160 Victoria Street, London, UK.
[1]Present address: Camino Las Flores 9806, Las Condes, Santiago, Chile

Corresponding author: Frances J. Cooper (frances.cooper@ucl.ac.uk)

Abstract

Crustal exhumation is central to mountain building, weathering, and sediment production processes, which significantly influence the composition and behavior of Earth’s oceans and atmosphere. It also controls the formation, enrichment, and preservation of porphyry copper deposits, which are a vital source of metals for the clean energy technologies underpinning the global green energy transition. Exhumation rates are typically determined from rock cooling histories combined with a geothermal model. However, in magmatically active regions, models can overpredict exhumation rates because the elevated heat signature is mistakenly attributed to advection driven by rapid exhumation. We present a method to accurately constrain exhumation histories in magmatic terranes that combines thermokinematic modeling of thermochronometric cooling histories with independent geobarometric constraints on the total exhumed crustal thickness. Focusing on the Central Andes, which has a prolonged history of magmatic and magmatic-hydrothermal activity, we find that accounting for this additional source of heat results in exhumed crustal thicknesses within error of the independent constraints, whereas ignoring it results in exhumed thicknesses up to four times greater than geologically plausible.

Keywords

Exhumation, thermochronometry, geobarometry, Central Andes, porphyry copper deposits, magmatic heat.

1. Introduction

Crustal exhumation is a fundamental process in active orogenic systems that continuously exposes fresh rock at the surface to be weathered, transported, and deposited as synorogenic sediments (Ring et al., 1999). This continuous breakdown and redistribution of material has significant implications not only for tectonic and surface processes, but also Earth's climate because chemical weathering influences atmospheric CO_2 and increased sediment loads in rivers, deltas, and oceans can impact biological productivity and carbon sequestration (e.g. Bufe et al., 2024; Galy et al., 2015; Hilton and West, 2020; Lee et al., 2015). Rapid exhumation is often linked to surface uplift, which creates high, expansive mountain ranges that can also affect the climate by altering wind patterns, precipitation, and global weathering rates (e.g. Kober et al., 2006; Ruddiman, 1997). It is therefore vital to build accurate global records of exhumation to assess how tectonic-climate coupling, and exhumation-driven rock uplift and sedimentation have affected Earth's climate in the past and may influence it in the future.

Exhumation rates have also been recognized to play an important role in controlling the formation, enrichment, and preservation of porphyry copper deposits in magmatic terranes such as the Central Andes, Southwest USA, New Guinea, and the Philippines (e.g. Dahlström et al., 2022; Evenstar et al., 2025; Sanchez et al., 2018; Sillitoe, 2010). As the global demand for metals such as copper accelerates to meet green energy targets, constraining spatial-temporal patterns of exhumation in magmatic terranes will be fundamental to exploration efforts, particularly during the preliminary high-risk terrane-scale phase.

Low-temperature thermochronometry is an effective tool for determining long-term exhumation rates when the temporal and spatial evolution of the geothermal gradient can be estimated (e.g. Ehlers, 2005 and references therein; Fox and Shuster, 2020; Furlong et al., 2021; Nguyen et al., 2022). Consequently, thermal models have become increasingly important in determining long-lived exhumation histories in orogenic systems such as the Himalaya (e.g.

Adams et al., 2015; Schultz et al., 2017; Thiede and Ehlers, 2013), the Alps (e.g. Glotzbach et al., 2011; Valla et al., 2012), and the Andes (e.g. Avdievitch et al., 2018; Schildgen et al., 2009; Stalder et al., 2020). However, a prolonged history of Andean magmatism makes it difficult to resolve thermal histories from low-temperature thermochronometers because heat has been transported both by exhumation-driven advection and the emplacement of igneous intrusions (e.g. Ehlers, 2005; Murray et al., 2018). Currently, most thermal models would interpret the elevated heat signature from an igneous intrusion as a high exhumation rate without recognizing the significance of the magmatic heat input. This means that exhumation rates, and consequently, total exhumed crustal thicknesses can be considerably overestimated.

Here, we demonstrate the importance of considering magmatic heat when using thermochronometry data to constrain exhumation rates in magmatic terranes. We also show that independent constraints on the total exhumed crustal thickness provide a vital check on model results, ensuring that predicted exhumation histories are geologically plausible. To do this, we re-evaluate the exhumation history of the western margin of the Central Andes in northern Chile by combining biotite $^{40}Ar/^{39}Ar$, zircon (U-Th)/He, and apatite (U-Th-Sm)/He cooling ages of exhumed intrusive rocks with a modified version of the thermokinematic modeling software, Pecube-D (Braun, 2003; Ehlers, 2023), that incorporates magmatic heat. Independent constraints on exhumation are provided by (1) published zircon U-Pb crystallization ages and Al-in-hornblende geobarometry pressures, which pinpoint the time and depth of emplacement and limit the total crustal thickness that could have been exhumed; and (2) cover rocks, which constrain the time by which rocks must have reached the surface (Dahlström et al., 2022). We find that without the addition of magmatic heat, models generate erroneously high exhumation rates, which result in exhumed crustal thicknesses up to four times greater than independent constraints allow. The framework we present here provides a crucial step forward to accurately constrain exhumation histories in magmatic terranes without the need to avoid samples that may have experienced thermal activity from igneous intrusions.

1.1 Exhumation and magmatism in the Central Andes

Continuous subduction of the oceanic Farallon-Nazca plate beneath South America since the Jurassic has resulted in the formation of the magmatically and volcanically active Andean orogen, stretching ~9,000 km along the western margin of the continent (Coira et al., 1982; Martinod et al., 2010). Second only to the Himalayan-Tibetan orogen in size and elevation, the Central Andes, which straddle the Chile-Peru border and encompass parts of Bolivia and Argentina, define the widest (~400 km) and highest (average elevation ~4 km) part of the system (Garzione et al., 2008). Progressive eastward migration of magmatism and deformation has also resulted in a series of margin-parallel, eastward-younging magmatic arcs, with active volcanism focused along the Western Cordillera on the edge of the Andean Plateau (Fig. 1) (Charrier et al., 2007; Haschke et al., 2006).

The majority of tectonic shortening, crustal thickening, rock uplift, and exhumation within the Central Andes began in the Paleocene to middle Eocene (~60–40 Ma; Barnes and Ehlers, 2009; McQuarrie et al., 2005), and has migrated progressively eastwards over time (Armijo et al., 2015; Reiners et al., 2015). In northern Chile, the main phase of rock uplift and exhumation occurred during the middle Eocene-Early Oligocene Incaic Orogeny (~45–33 Ma; Mpodozis and Cornejo, 2012; Tomlinson et al., 2001), which has been linked to a period of increased convergence (Pardo-Casas and Molnar, 1987). The Incaic Orogeny also coincided with a major phase of magmatic-hydrothermal activity (~45–31 Ma), which generated a rich belt of porphyry copper deposits along the Andean foothills (the “Precordillera”) associated with margin-parallel strike-slip faulting on the Domeyko fault system (Mpodozis and Cornejo, 2012 and references therein) (Fig. 1).

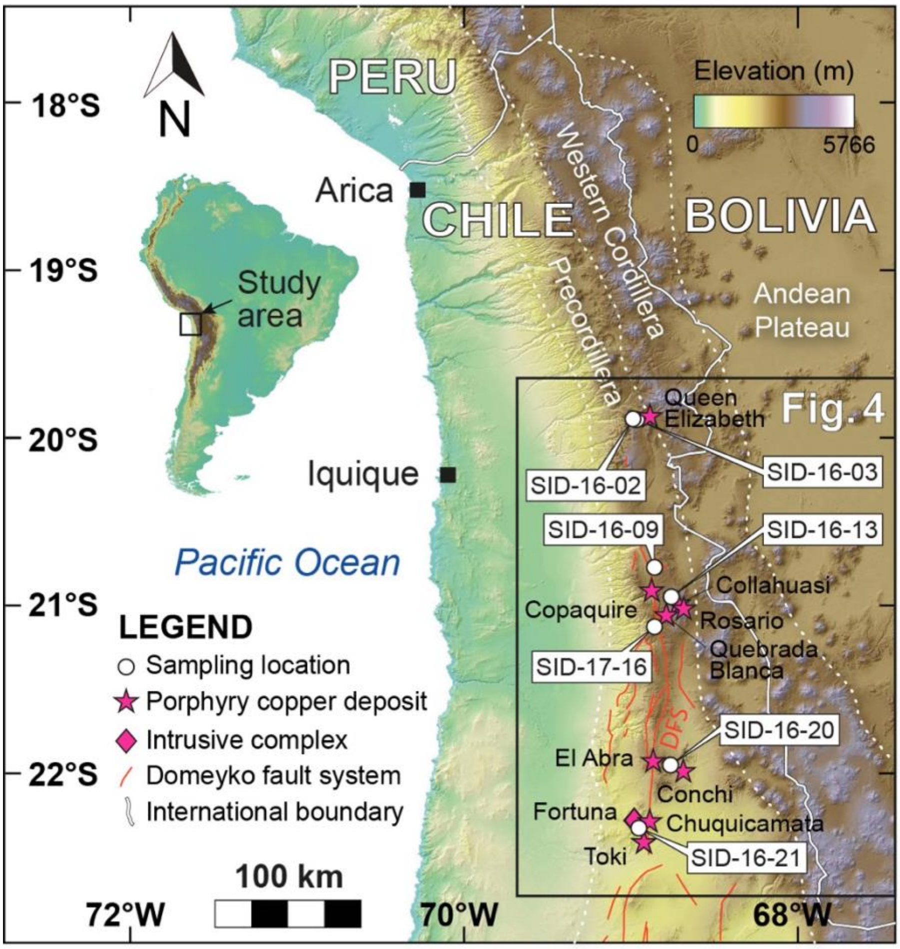

Figure 1. Digital elevation model of the Central Andes highlighting relative positions of the Andean Plateau, Western Cordillera, and Precordillera. Porphyry copper deposits and intrusive complexes of the middle Eocene-Early Oligocene metallogenic belt lie along the Domeyko fault system (DFS) within the Precordillera. Inset box corresponds to the area shown in Figure 4 and shows sampling locations within the area of study.

The Central Andes are also one of the driest places on Earth, with hyperaridity thought to have persisted since at least the middle Miocene (Amundson et al., 2024; Cooper et al., 2016; Rech et al., 2019; Shaw et al., 2021 and references therein). Long-term exhumation rates, derived primarily from low-temperature thermochronometry, are correspondingly low. Estimated mean exhumation rates in the Precordillera range from <0.2 km/Myr since ~50 Ma (Avdievitch et al., 2018) to 0.25 km/Myr since ~80 Ma (Stalder et al., 2020), approximately an order of magnitude lower than the highest rates recorded in the Himalaya (e.g. Adams et al., 2015; Thiede and Ehlers, 2013). During the Incaic Orogeny, exhumation rates are estimated to have reached 0.1–0.4 km/Myr (Dahlström et al., 2022; Maksaev and Zentilli, 1999), before slowing to ~0.02–0.09 km/Myr since the early Oligocene (Maksaev and Zentilli, 1999; Sanchez et al., 2018; Shaw et al., 2021), and <0.001 km/Myr over the past ~6 million years (Kober et al., 2007).

However, estimates of Central Andean exhumation derived solely from low-temperature thermochronometry either have not accounted for the presence of magmatic heat or deliberately avoided collecting or interpreting samples that are suspected to have been affected by magmatic or hydrothermal activity (e.g. Reiners et al., 2015). The presence of magmatic-hydrothermal porphyry copper systems is particularly problematic as they are characteristically associated with shallow intrusions (Sillitoe, 2010), and thus have the ability to significantly perturb the geothermal gradient.

1.2 Exhumation, magmatism, and the geothermal gradient

The form of a 1-D geothermal gradient in the shallow crust is primarily a function of the flux of heat from depth, the rate at which rocks move toward the surface, the production of radiogenic heat, and the transmission rate of heat through the rocks (thermal diffusivity). This combination of processes and conditions leads to non-linear geothermal gradients where the rate of heat production is high or where exhumation is fast enough for rocks to move heat from depth more quickly than it can be dissipated through conduction (Stüwe et al., 1994). This effect is evident in Figure 2A, where the geothermal gradient becomes increasingly non-linear as the exhumation rate increases. At higher exhumation rates, rocks can advect more heat and – without a commensurate change in thermal diffusivity – the shallowest portion of the gradient increases significantly.

Another mechanism for advecting heat into the shallow crust is via the intrusion of magmatic bodies (e.g. Murray et al., 2018). While heat advection due to exhumation produces a curvilinear thermal profile, the intrusion of magma will produce a tabular perturbation within the curved field (Fig. 2B). The tabular form of the intrusive heat remains defined while the intrusion is active. The shallow geothermal gradient becomes exceptionally high when shallow intrusions are active, but once the magmatic event ceases, it relaxes back to a curvilinear form as conduction disperses the heat. Notably, once the intrusions have crystallized and begun to cool, the elevated geothermal gradient may be difficult to discern from a gradient resulting from a period of relatively rapid exhumation.

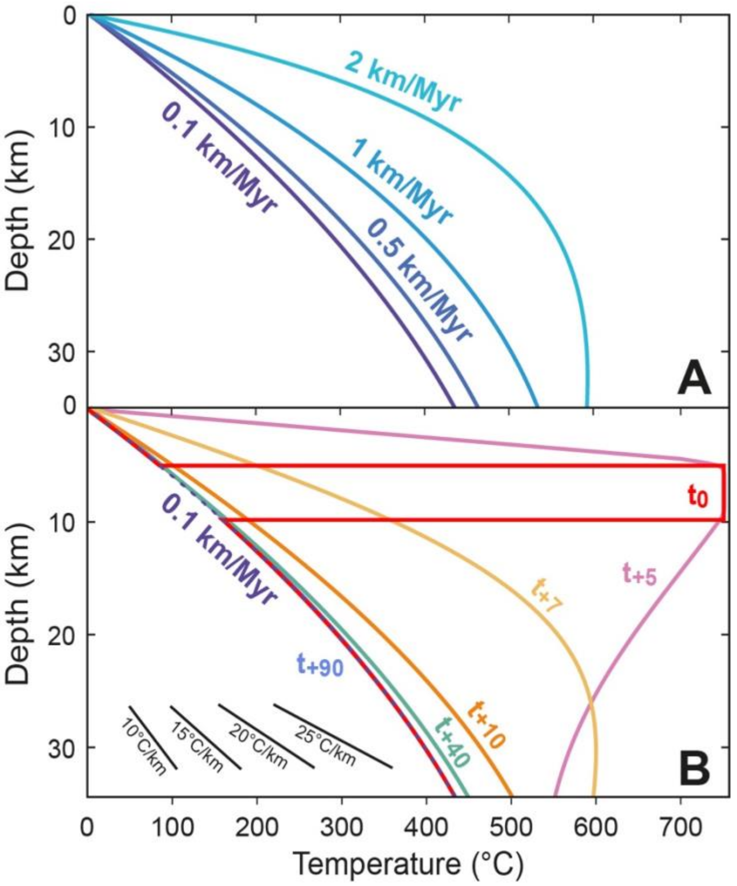

Figure 2. 1-D models illustrating variations in geothermal gradient as a function of exhumation rate and magmatic heat. (A) An increase in exhumation rate advects more heat to the surface, causing the shallow geothermal gradient to steepen. Curves denote the geotherms for the transient solutions of the heat transfer equation for different steady exhumation rates. **(B)** Intrusion of a 5 km-thick magmatic body at 5 km depth during slow exhumation at 0.1 km/Myr also causes the geothermal gradient to steepen. When the intrusion is held at a constant temperature of 750°C for 5 Myr and then allowed to cool, the following thermal evolution is observed: Initially (t_0), the gradient is severely perturbed by the intrusion but 5 Myr after the intrusion event has ceased (t_{+10}), gradual diffusion of heat results in a smooth elevated gradient virtually indistinguishable from one caused by an increased exhumation rate (c.f. 0.5 km/Myr curve in A). After 40 million years (t_{+40}), the gradient has almost returned to its initial unperturbed state and after 90 million years (t_{+90}) there is no trace of the magmatic heat pulse. Model parameters are listed in Table S5.

Magmatism can considerably complicate the interpretation of exhumation histories derived from thermochronometry. First, the elevated temperatures produced by intrusions can partially or completely reset chronometers, thus removing or modifying any previous record of cooling (Murray et al., 2018). When the magmatic activity ceases, the elevated isotherms will descend rapidly through the crust, creating a situation in which chronometers with different closure temperatures may give the same age, suggesting a very rapid cooling rate. Second, most 1-D thermokinematic models assume monotonic cooling induced by exhumation of rocks to the surface, and as such are only able to account for a variation in cooling rate by changing the exhumation rate (assuming other boundary conditions remain constant). However, it is ultimately the thermal history rather than the geothermal gradient that governs the thermochronometric record, and thermal histories themselves can be non-unique. Different combinations of exhumation, heat advection, and transient magmatic inputs may produce indistinguishable cooling paths and similar ages. Geological constraints are therefore essential for narrowing the range of plausible thermal–exhumation histories in regions affected by magmatism. It follows that in terranes where shallow intrusions are known or suspected, more effort is needed to constrain the thermal inputs of magmatic event(s) and to include these additional sources of heat into a thermal model when attempting to constrain exhumation rates based solely on thermochronometry.

Dahlström et al. (2022) employed an alternative approach – not reliant on thermal histories – to constrain exhumation rates within the Central Andean Precordillera. Zircon U-Pb crystallization ages of granitoid intrusions along a ~730 km-long arc-parallel transect in northern Chile (~18°–24°S) were combined with emplacement depths from Al-in-hornblende geobarometry (Mutch et al., 2016) to determine (1) the total thickness of exhumed crust, and (2) the average exhumation rate from emplacement at depth to exposure at the surface. Exhumation rates were further refined using the ages of overlying cover rocks or the timing of weathering and enrichment of copper deposits, which provided a minimum constraint on when the intrusions must have reached the surface. This revealed two phases of exhumation in the early Permian-middle Triassic and middle Eocene-late Oligocene, with an intervening period of burial, consistent with previous sedimentology and thermochronology studies of the Central

Andes (e.g. Armijo et al., 2015; Avdievitch et al., 2018; Michalak et al., 2016). The highest exhumation rates, coincident with the Incaic Orogeny, ranged from ~0.1–0.4 km/Myr, consistent with estimates from low-temperature thermochronometry (Avdievitch et al., 2018; Maksaev and Zentilli, 1999; Stalder et al., 2020). However, these average exhumation rates only provide a simplified picture of the exhumation history from emplacement to surface exposure and may hide important variations in exhumation over time.

1.3 A re-evaluation of Central Andean Exhumation from shallow granitoid intrusions

Dahlström et al. (2022) found consistently shallow pluton emplacement depths of ~4–6 km, suggesting a major influence on the shallow geothermal gradient within and near these intrusions, and therefore on exhumation rate estimates based on thermochronometry. To test the sensitivity of exhumation histories to the heat of shallowly-emplaced intrusions, we build on the dataset of Dahlström et al. (2022) by adding new themochronometric constraints within a thermokinematic model framework that includes magmatic heat. Focusing on a subset of seven Eocene samples (Fig. 1, Table S1) representing emplacement and exhumation during the Incaic Orogeny, we performed zircon (U-Th)/He (ZrnHe), apatite (U-Th-Sm)/He (ApHe), and biotite ^{40}Ar/^{39}Ar (BtAr) analyses to establish cooling histories between emplacement and surface exposure (Fig. 3). The emplacement depth of each sample provides an independent constraint on the maximum thickness of crust that could have been exhumed, allowing us to refine our model results to only accept exhumation histories that satisfy this criterion. This is particularly useful in magmatically active regions where rapid cooling after an intrusion event can be mistakenly interpreted as signaling a high exhumation rate, resulting in excessive estimates of crustal exhumation.

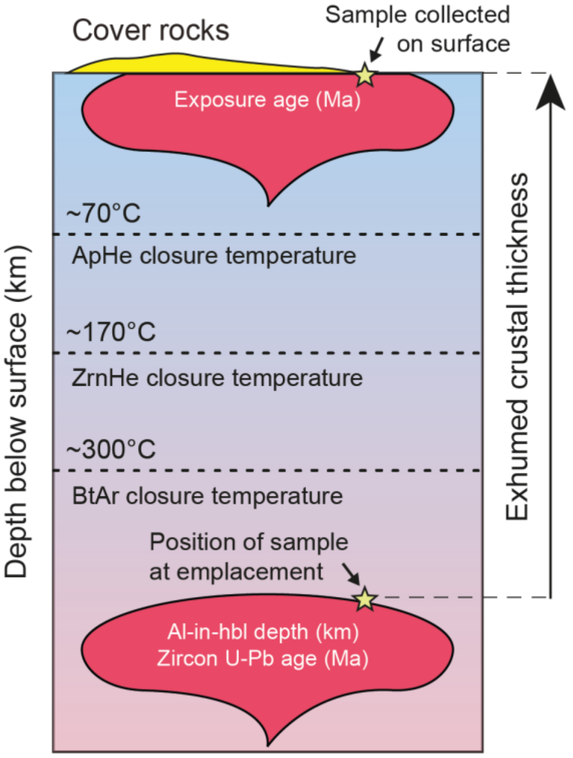

Figure 3. Schematic representation of the upper crust showing how the exhumation history of an intrusion is determined by combining mineral cooling ages with independent constraints on the depth and timing of emplacement and surface exposure. The emplacement depth provides a maximum constraint on the total exhumed crustal thickness that cannot be exceeded in model results. Closure temperatures follow Farley (2000); Reiners et al. (2004); Schaltegger et al. (2019); and van Soest et al. (2011).

2. Thermochronometric constraints on mineral cooling histories

2.1 Zircon (U-Th)/He and Apatite (U-Th-Sm)/He dating

Zircon and apatite grains from all seven samples were separated using conventional sieving, magnetic, and heavy liquid mineral separation techniques. Five apatites and five zircons from each sample were then handpicked for analysis, targeting euhedral grains with a short axis no less than 80 µm where possible. Selected apatites were inclusion-free, while inclusions in zircons were kept to a minimum. For each grain, the dimensions required for an alpha particle ejection correction were measured, after which the grains were loaded into niobium microcrucibles for analysis in the Group 18 Laboratories at Arizona State University. Full analytical details and data reduction procedures are provided in the supplementary material. For complete zircon (U-Th)/He and apatite (U-Th-Sm)/He data, see Tables S2 and S3.

2.2 Biotite $^{40}Ar/^{39}Ar$ dating

Single crystal incremental heating experiments were performed on biotite from samples SID1602, SID1613, SID1620, and SID1716 (Table 1). Biotite separates were sent to the Oregon State University reactor for irradiation prior to $^{40}Ar/^{39}Ar$ analysis in the WiscAr Laboratory at the University of Wisconsin-Madison. Full analytical details and data reduction procedures are provided in the supplementary material. For complete $^{40}Ar/^{39}Ar$ data, see Table S4 and Figure S1.

2.3. Results and interpretation

BtAr, ZrnHe, and ApHe ages (Figs 4B and S1, Tables 1 and S1–S4.) suggest a main phase of cooling in the middle Eocene to late Oligocene, coincident with the Incaic Orogeny. BtAr ages of ~43–36 Ma for four of the seven samples are consistently ≲2 Myr younger than zircon U-Pb (ZrnUPb) crystallization ages (~45–37 Ma), suggesting exceptionally fast post-emplacement cooling from ~800°C to ~300°C, at rates >100°C/Myr (Fig. S2), consistent with steep magmatic cooling trajectories documented by Schaltegger et al. (2019). ZrnHe ages for all seven samples range from ~37.6 Ma to ~30.2 Ma, with four samples tightly clustered around ~33.7–33.2 Ma, which is shortly after a pulse of late Eocene magmatism and porphyry copper mineralization in the region (Fig. 4, Table S9), suggesting possible thermal resetting. ApHe ages for samples SID1602 and SID1603 of ~24.3 Ma and ~24.4 Ma are within error of the overlying volcanic cover unit, suggesting that they may have been thermally reset by it. However, a similar age of ~24.6 Ma for sample SID1609 is significantly different enough from its 16.6 Ma cover unit to assume that it was not thermally reset. The remaining four samples give ApHe ages of ~31.7–29.3 Ma, reflecting a major phase of middle Oligocene cooling just after the cessation of main Incaic orogenesis.

Table 1. Geobarometry, geochronology, and thermochronology data

Sample	Depth (km)	2σ (km)	ZrnUPb (Ma)	2σ (Ma)	BtAr (Ma)	2σ (Ma)	ZrnHe (Ma)	2σ (Ma)	ApHe (Ma)	2σ (Ma)	Exp (Ma)	2σ (Ma)	Ref
SID1602	6.00	0.64	40.65	0.30	38.64	0.08	30.2	2.7	24.3	3.5	25.7	1.0	(Sellés et al., 2016)
SID1603	5.58	0.77	40.14	0.19	-	-	31.4	2.0	24.4	0.7	25.7	1.0	(Sellés et al., 2016)
SID1609	5.10	0.42	45.61	0.31	-	-	33.7	4.8	24.6	4.1	16.6	1.1	(Tomlinson et al., 2001)
SID1613	4.92	0.57	45.03	0.33	43.28	0.13	33.8	3.2	31.7	2.4	16.6	1.1	(Tomlinson et al., 2001)
SID1620	5.20	1.10	36.80	0.24	36.18	0.09	33.3	2.5	29.5	4.9	13.1	0.2	(Perelló, 2003)
SID1621	4.43	0.67	42.21	0.12	-	-	37.6	5.7	29.3	0.9	20.8	1.2	(Sillitoe and McKee, 1996)
SID1716	5.91	0.54	44.49	0.34	42.21	0.16	33.2	0.5	31.1	3.1	5.8	0.4	(Tomlinson et al., 2001)

Abbreviations: Depth = Pluton emplacement depth; ZrnUPb = Zircon U-Pb age (from Dahlström et al., 2022); BtAr = Biotite $^{40}Ar/^{39}Ar$ age; ZrnHe = Zircon (U-Th)/He age; ApHe = Apatite (U-Th-Sm)/He age (this study); Exp = Minimum age for surface or near-surface exposure (with appropriate reference). See supplementary material for analytical details and full datasets.

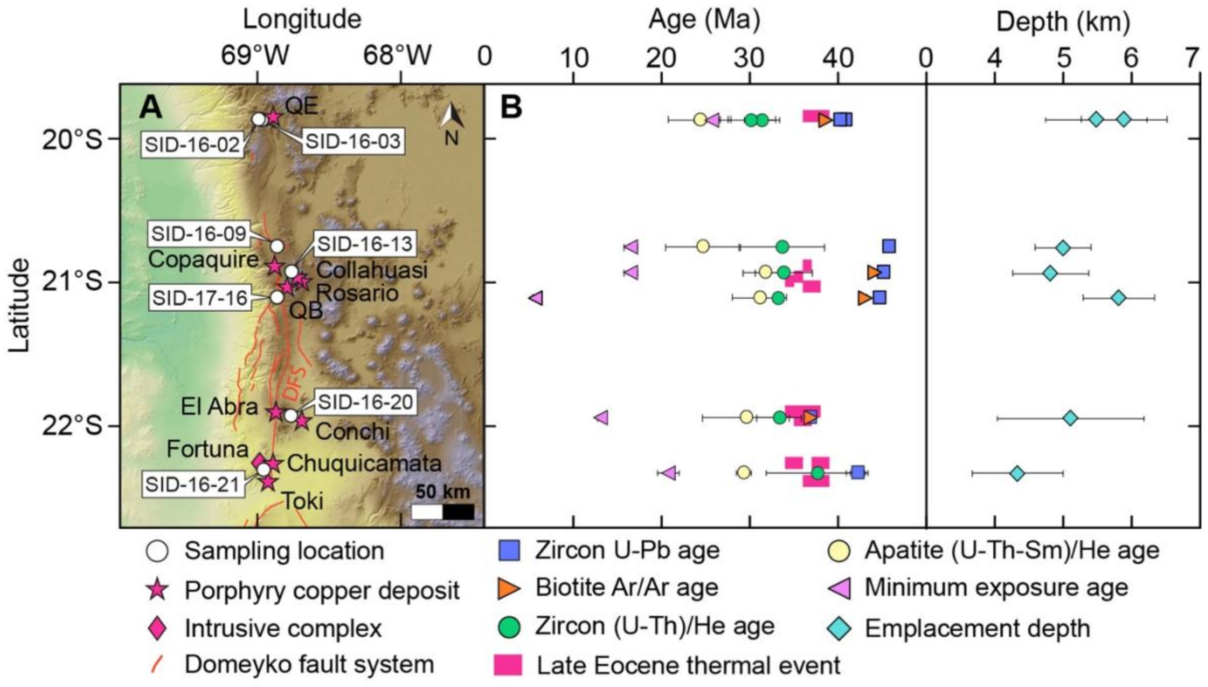

Figure 4. (A) Sampling locations and heat sources of late Eocene age within the study area. See Figure 1 for regional context. QE = Queen Elizabeth; QB = Quebrada Blanca. (B) Geochronology,

thermochronometry, and geobarometry constraints on the emplacement, cooling, and exposure histories of the samples shown at the 2σ confidence level. Overlapping apatite (U-Th-Sm)/He ages and minimum exposure ages plus younger zircon (U-Th)/He ages for samples SID1602 and SID1603 suggest thermal resetting by overlying volcanic cover rocks, so they were excluded from the thermokinematic modeling. Age ranges for late Eocene heating associated with porphyry copper deposits and intrusive complexes derive from a compilation of dated intrusions listed in Table S9.

3. Exhumation histories from thermokinematic modeling

3.1 Modeling approach

We assume that the thermal evolution of our samples was primarily controlled by two independent geologic processes: exhumation and magmatism. Therefore, to track their movement toward the surface while simultaneously accounting for the transient geotherm, we employ the thermokinematic modeling software, Pecube-D (Ehlers, 2023). Plausible exhumation histories were determined using a modified version of the software that accounts for the presence of magmatic heat. Due to the shallow level of emplacement, we only consider heat flow in the vertical direction and thus run the model in 1-D by restricting the flow of heat laterally. This means we only constrain the vertical component of exhumation. To put our results into context with previous Central Andean studies, we use the same model parameters (e.g., fixed base temperature, crustal density, conductivity, and radiogenic heat production; Table S5); but to ensure they are the most appropriate values, we performed sensitivity analyses to understand the extent to which variations might affect our model results (see supplementary material for details). We conclude that while the model parameters place important constraints on our plausible results by controlling the shape of the geotherm (Fig. 2), they have considerably less influence than the velocity histories or magmatic heating.

Our approach is based on the well-established 1-D Monte Carlo method (Adams et al., 2015; Thiede and Ehlers, 2013) in which possible exhumation histories are forward modeled to produce predicted cooling ages that can be compared to our observed mean cooling ages and their standard errors using the χ^2 criterion (see supplementary material for details). In addition to our requirement that each chronometer is predicted with statistical rigor, we also require that the integral of plausible exhumation histories predict the independently constrained pluton emplacement depths using the χ^2 criterion (Fig. S3).

3.2 Adding magmatic heat

Within the study area, our samples record two significant periods of magmatic activity. Firstly, the middle–late Eocene emplacement of the shallow granitoid intrusions themselves (Dahlström et al., 2022). Secondly, a late Eocene phase of magmatic and magmatic-hydrothermal activity associated with porphyry copper mineralization across the region (Fig. 4B; Table S9 and references therein), which we suspect to have reset the ZrnHe ages. We expect that the thermal histories of our samples record the combined effects of both thermal events while simultaneously undergoing exhumation.

To simulate the emplacement of a magmatic intrusion in our 1-D models we determine the depth to the top and bottom of the heat pulse, the temperature of the pulse, and its initiation and duration. This is similar to the way dikes and sills have been modeled previously (e.g. Ehlers, 2005). A tabular pulse of heat is added to the crust that perturbs the geotherm, which is then allowed to evolve as the crustal package is exhumed. Once the thermal event is over, the heat pulse is switched off and the geotherm continues to evolve without the additional heat source. The thickness, temperature, and duration of the intrusion yield the total amount of heat generated in excess of exhumation-driven advection, which is then dissipated over time by flowing out of the top of the model.

To determine the thickness and duration of the primary granitoid intrusions, we estimated the volume of each sampled pluton from mapped surface expressions and empirical relationships between length, width, and thickness (Cruden et al., 2017; McCaffrey and Petford, 1997). Combining the calculated volumes with magma flux rates from Matzel et al. (2006), we estimated intrusion durations, which were initiated at the ZrnUPb crystallization age of each sample (Dahlström et al., 2022). Murray et al. (2018) used a similar method for incorporating magmatic heat into thermal models, and we follow their use of 750°C for the intrusion temperature, which accounts for the prolonged history of intrusion building and the effects of latent heating. Given the average size of the sampled intrusions and a flux rate of 2.0 × 10−4 km^3yr^{-1} (Matzel et al., 2006), we use the following parameters for our primary intrusions: 5 km thick, top is 5 km deep (based on the average emplacement depth from Dahlström et al. (2022)), a consistent temperature of 750°C, and a cessation time of 2.8 Myr after initiation. See supplementary material for full details.

Simulating the subsequent late Eocene thermal event associated with porphyry copper mineralization is more difficult because the precise locations, dimensions, and emplacement mechanisms of the intrusions that may have affected our samples are unknown. On the basis that porphyritic intrusions form within the upper 5 km of the crust (Sillitoe, 2010), we used a conservative emplacement depth of 5 km, consistent with the primary granitoid intrusions. Since they are typically small stocks and dikes with diameters and lengths ≤ 1 km (Sillitoe, 2010), we adopted a consistent thickness of 1 km in each model. A moderate temperature of 400°C was used to account for the lower temperature of these magmatic-hydrothermal systems

(~300–650°C; Cernuschi et al., 2023) and the fact that the presence of hydrothermal fluids could reduce the extent of the thermal aureole (Abbey et al., 2024). The thermal longevity of these systems is also poorly constrained, but magmatic-hydrothermal activity is typically thought to last <1–5 Myr (e.g. Li et al., 2012; von Quadt et al., 2011). A thermal pulse lasting 0.45 Myr was deemed reasonable as it is consistent with the <1–5 Myr duration of these systems and does not reset the older thermochronometers within our samples. To set initiation times, we used the timing of mineralization from the nearest known ore bodies in the region (Table S9). Model setups for each sample are provided in Table S10.

It is not our intention to use our thermochronometry data to constrain specific magmatic or magmatic-hydrothermal processes to avoid an overinterpretation of results. Therefore, we use the same parameterization for each of the primary and secondary intrusions in every model, while allowing for some regional variation based on initialization times from crystallization or mineralization ages. While it is unlikely that each of the intrusions had the same physical and thermal structure, we consider this to be a conservative approach as it attempts to reduce the number of unconstrained parameters.

3.3 Model results

3.3.1 Exhumation histories without magmatic heat

When magmatic heat is not accounted for, model solutions for all samples can be found simply by varying exhumation rates over time. However, the absence of magmatic heat means that models predict higher exhumation rates to cool these rocks more quickly. Rapid exhumation creates high geothermal gradients before ApHe closure, which then requires a significant slowdown in exhumation for the appropriate cooling ages to be preserved at the surface rather than lost to erosion (Fig. 5). A consistent pattern of exhumation emerges from model solutions that do not include magmatic heat in which rates increase after BtAr closure and then decrease dramatically by up to an order of magnitude after ZrnHe closure (Fig. 5A).

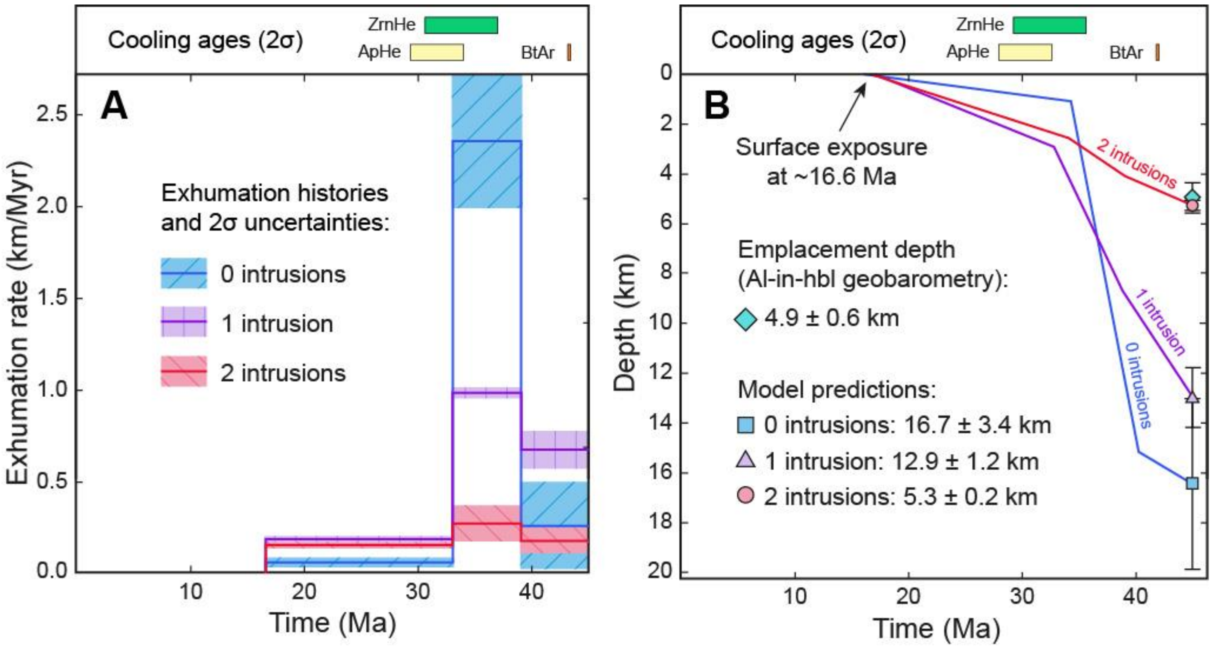

Figure 5. Predicted exhumation histories and exhumed crustal thicknesses for sample SID1613 in models run with 0 intrusions, 1 intrusion, and 2 intrusions. To reproduce the observed cooling ages without the addition of magmatic heat, the model predicts exhumation rates up to 2.36 ± 0.37 km/Myr (A), which requires the removal of 16.7 ± 3.4 km of crust since the time of emplacement (B). This is 3.4x greater than the ~4.9 km emplacement depth of the sample. Addition of magmatic heat from a single intrusion (5 km thick, 750°C for 2.8 Myr) requires exhumation rates as high as 0.99 ± 0.03 km/Myr, leading to the removal of 12.9 ± 1.2 km of crust, which is 2.6x the emplacement depth. When a second intrusion is added (1 km thick, 400°C for 0.45 Myr), rates up to only 0.27 ± 0.1 km/Myr are required. This reduces the removal of crust to just 5.3 ± 0.2 km, which is within error of the emplacement depth.

Exhumation rates predicted between the closure of ZrnHe and ApHe (~0.7–2 km/Myr from ~34 Ma to ~29 Ma) are unusually high given that rates of this magnitude are not observed anywhere in the orogen around this time. In addition, exhumation rates of these magnitudes, even for relatively short periods of time would result in significant erosional unroofing, well beyond what can be accounted for by the independent intrusion emplacement depths (Dahlström et al., 2022). In other words, it is not possible to exhume an intrusion from a depth greater than its emplacement depth. For these reasons we consider these exhumation histories to be geologically implausible even though they can produce thermal histories that fit our observed cooling ages.

3.3.2 Exhumation histories with magmatic heat

As demonstrated in Figures 5 and 6, the largest difference between exhumation histories derived from models without and with magmatic heat input is that the latter do not require unusually high exhumation rates before the closure of ApHe. If the primary intrusion is included, the total required exhumed crustal thickness is greatly reduced but does not match the independent values from the intrusion emplacement depths (Fig. 5B). If a second heat pulse is added, the predicted exhumation rates and exhumed thicknesses are further reduced and predicted exhumation histories closely match independent estimates of total exhumed crust (Figs 5 & 6).

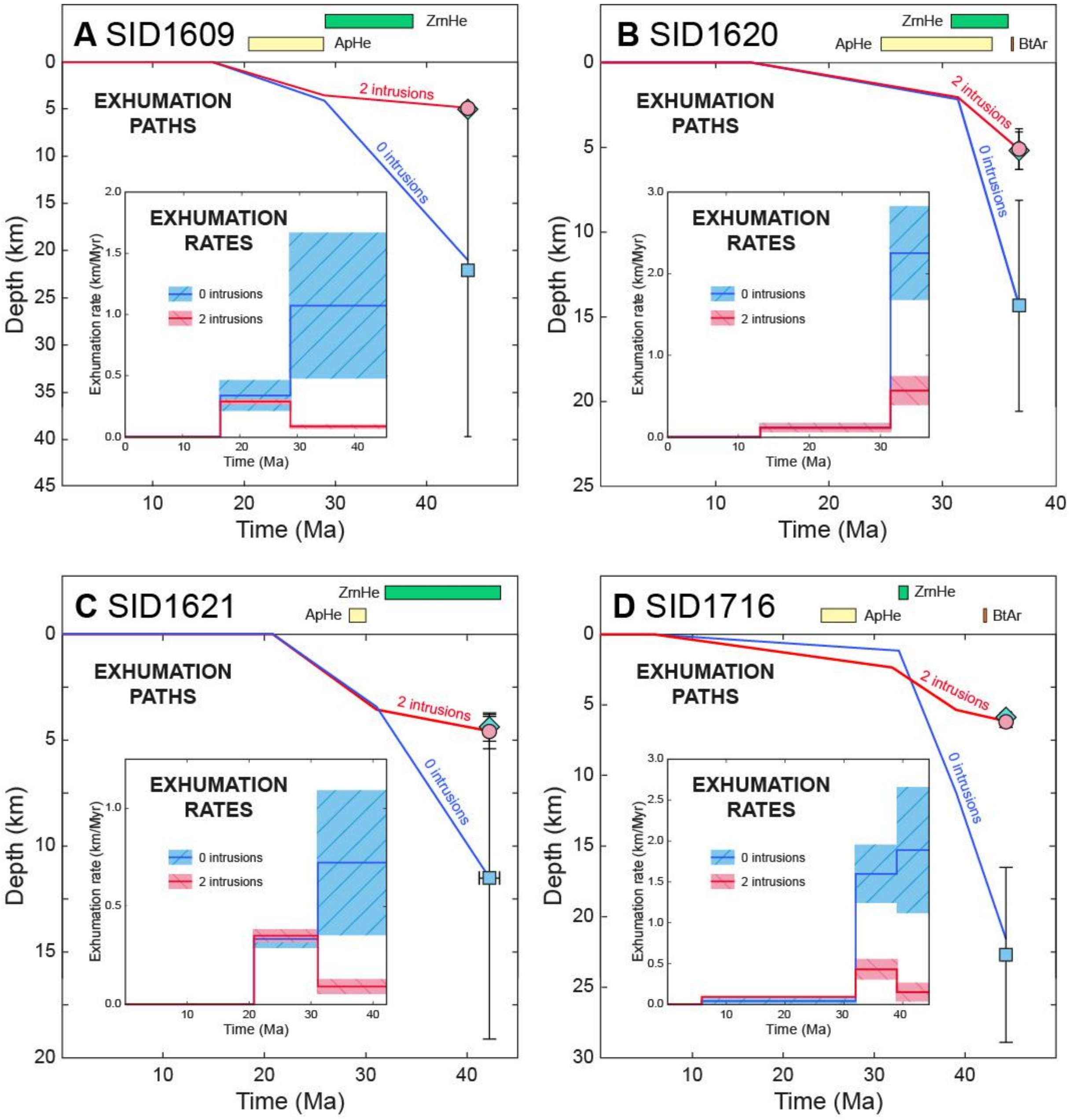

Figure 6. Model predicted exhumation histories and observed cooling ages for samples (A) SID1609, (B) SID1620, (C) SID1621, and (D) SID1716 comparing scenarios with 0 intrusions and 2 intrusions. In each case, exhumation paths are determined from the average predicted exhumation rates. Symbology follows Figure 5.

4. Discussion

4.1 The importance of considering magmatic heat

Thermal models can readily produce non-unique exhumation histories for the same dataset. This is because velocity histories with different configurations can produce similar geothermal gradients over the course of the modeled history. Relatively older cooling ages may record slow movement within an elevated geothermal gradient or rapid movement within a gentle geothermal gradient. A near infinite combination of cooling rates and geothermal gradients can produce a given cooling age, unless the geothermal gradient prior to system closure is well-constrained independently of the chronometric system in question. However, not all these combinations will be geologically plausible. For this reason, models with additional constraints from independent observations can produce a narrower range of results. The known geologic history of the western margin of the Central Andes requires that thermokinematic models incorporate magmatic heat sources when analyzing intrusive samples.

Using a modified version of Pecube-D that incorporates magmatic heat, combined with independent geobarometry constraints and a multichronometer approach, we have demonstrated that (1) predicted exhumation rates can be an order of magnitude higher when magmatic heat is not taken into account, (2) the total exhumed crustal thickness can be up to four times greater than independent geobarometry constraints allow (Fig. 7, Table S11), and (3) constraining the elevated geothermal gradient resulting from active magmatism prior to closure of thermochronometers is critical to informing long-term exhumation histories in magmatic terranes.

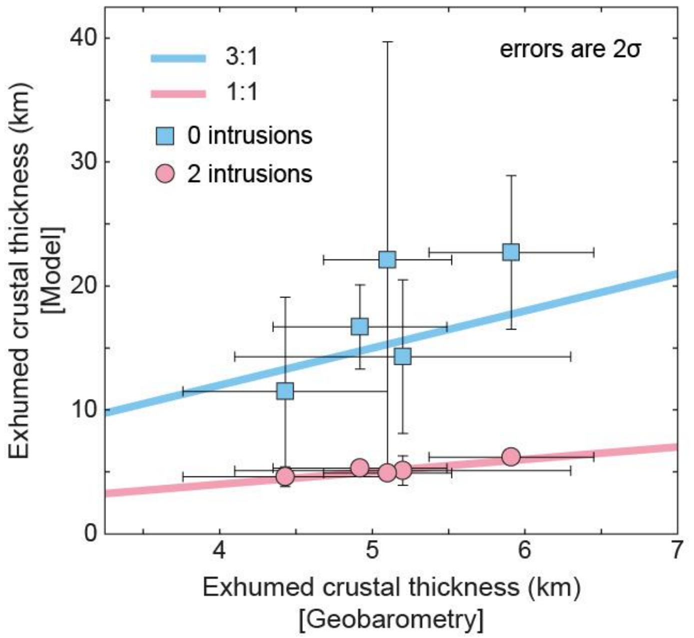

Figure 7. A comparison between exhumed crustal thickness determined from geobarometry and predictions from Pecube-D modeling for scenarios with and without magmatic heat. Models incorporating two magmatic heat pulses lie close to a 1:1 line whereas models with no magmatic heat input consistently overestimate the exhumed crustal thickness by an average factor of three, but reaching up to four times greater than geologically plausible. Note that the 1:1 line (pink) and 3:1 line (blue) are reference lines and not regressions through the datasets.

It is important to emphasize that we are not using this model to precisely replicate magmatic or magmatic-hydrothermal processes, which are more spatially and temporally complex than we have been able to represent. However, since our model is primarily governed by the established equations for heat flow (Carslaw and Jaeger, 1959) and the kinematic characteristics of specific chronometers, our results represent physically permissible and statistically plausible versions of exhumation and magmatic heat flow histories. Our ability to accurately model both the cooling ages and total exhumed crustal thickness for each sample suggests that the heat flux we include for each thermal event is a plausible representation, despite our highly simplified parameterization. The exact physical properties of intrusions are likely to vary from what we have modeled, but the parameters used are conservative values based on previous studies of intrusion dynamics that produce a total heat flux within the modeled history able to predict all our observations.

We find that nearly all our samples require an additional heat input to keep minerals warmer for longer such that their cooling ages are younger, while allowing for slower exhumation and minimizing exhumed crustal thicknesses. A notable exception is sample SID1621, which can produce plausible cooling histories and exhumed thicknesses by modeling relatively low exhumation rates of <1 km/Myr before the closure of ZrnHe. However, in this case, the 2σ uncertainty on the ZrnHe age is 15%, which is higher than the other samples due to a large dispersion in single crystal cooling dates, allowing for more variability in plausible exhumation histories. We also note that this sample has no BtAr cooling age, so it is not possible to accurately constrain the geothermal gradient before the closure of the poorly-constrained ZrnHe age. While this particular sample may appear problematic, we consider it to be an important example of how poorly-constrained models can yield difficult-to-interpret and non-unique solutions.

5. Broader implications

We have opted for a relatively simple simulation of magmatic events to minimize parameterization and to avoid overinterpreting our primary observations. Nevertheless, we provide a basis upon which more complex simulations can be built. Despite this simplification, the exhumation rates constrained here are consistent with previous findings in the Central Andes (Avdievitch et al., 2018; Dahlström et al., 2022; Kober et al., 2007; Maksaev and Zentilli, 1999; Sanchez et al., 2018; Shaw et al., 2021; Stalder et al., 2020). This is a positive sign that our modeling approach – when paired with independent constraints on the total exhumed crustal thickness – is valid and can be applied to other magmatic terranes, particularly those with a history of shallow magmatic activity.

Shallowly emplaced intrusions are common around the world and throughout geological history. They are often intruded as subvolcanic laccoliths such as the Permian Cornubian Batholith in Cornwall, UK (~5–6 km; Pownall et al., 2012), the Oligocene Henry Mountains in Utah (~3–3.5 km; Wilson et al., 2016), the middle Miocene Torres del Paine in Patagonia (~2–3 km; Michel et al., 2008), and the late Miocene Slaufrudalur pluton in Iceland (~1 km; Burchardt et al., 2012), or comprise epizonal stocks linked to magmatic-hydrothermal mineralization such as the Jurassic Yerington copper deposit in Nevada (Dilles, 1987), the Eocene Yulong copper-molybdenum deposit in Tibet (~4–5 km; Zhao et al., 2022), and the Pliocene Grasberg copper-gold deposit in Indonesia (<2 km; Weiland and Cloos, 1996). Published exhumation rate estimates for these systems are limited, but a thermochronometric study of Torres del Paine suggested rapid exhumation rates of up to 3 km/Myr without factoring in magmatic heat input (Muller et al., 2024). Exhumation of the Cornubian Batholith is poorly constrained, but its protracted cooling history is thought to reflect the addition of heat from multiple intrusive episodes (Chesley et al., 1993), which would need to be factored into any exhumation rate estimates. These examples highlight places where shallow intrusion-related reheating may masquerade as accelerated exhumation in thermochronologic records, underscoring the broader applicability of our approach in detecting and correcting for such magmatic biases. In such places, employing our approach would provide a more straightforward route to constraining long-term exhumation histories as there would be no need to avoid rocks suspected of being affected by magmatic or magmatic-hydrothermal activity.

6. Conclusions

We demonstrate that incorporating magmatic heat into thermal models is important when determining long-term exhumation histories in magmatically-active regions, particularly where shallow intrusions are known or suspected. The addition of heat from primary and secondary magmatic sources can generate total heat budgets similar to those resulting from high rates of exhumation, as recorded in the relatively coarse multichronometer cooling histories of our samples. With the addition of magmatic heat, thermal models predict lower exhumation rates, which reduces the total exhumed crustal thickness. Independent geobarometry constraints provide an important check on model results, ensuring that predicted exhumation histories are geologically plausible and exhumed crustal thicknesses are not exceeded.

Acknowledgements

This work was generously supported by BHP. We are also grateful to the Society of Economic Geologists for providing additional funding through a Hugh McKinstry Fund Student Research Grant awarded to S.I. Dahlström. We are indebted to Willi Kappler whose immense patience and perseverance ensured that the numerical modeling was successful, and to Michelle Aigner for her assistance with the (U-Th)/He and (U-Th-Sm)/He analyses. We thank Matthew Fox for comments on an earlier version of the manuscript, David Whipp and an anonymous reviewer for their constructive feedback, and Alex Webb for editorial handling.

Author contributions

F.J. Cooper: Conceptualization, Funding acquisition, Formal analysis, Investigation, Methodology, Visualization, Supervision, Writing – Original Draft, Writing – Review & Editing. **B.A. Adams:** Conceptualization, Formal analysis, Investigation, Methodology, Visualization, Supervision, Writing – Original Draft, Writing – Review & Editing. **S.I. Dahlström:** Conceptualization, Funding acquisition, Formal analysis, Investigation, Methodology, Writing – Review & Editing. **T.A. Ehlers:** Conceptualization, Formal analysis, Methodology, Supervision, Writing – Review & Editing. **M.C. van Soest:** Formal Analysis, Writing – Review & Editing. **K.V. Hodges:** Formal analysis, Writing – Review & Editing.

B.R. Jicha: Formal analysis, Writing – Review & Editing. **B.S. Singer:** Formal analysis, Writing – Review & Editing. **J. Cortes Yañez:** Investigation, Writing – Review and Editing. **R.J. Perkins:** Conceptualization, Methodology, Writing – Review & Editing.

Competing interests

The authors declare that they have no competing interests.

Data availability

All data are available in the main text or the supplementary materials. Pecube_D is available at https://zenodo.org/records/7785668 and Matlab codes are available at https://github.com/baadams/pecube.

References

Abbey, A.L., Randolph-Flagg, N., de Villa, K., Kim, S.L., Shuster, D.L., 2024. Tracing short-lived hydrothermal circulation systems and water-rock interactions around small-scale intrusions. Geochimica et Cosmochimica Acta 366, 113–127, doi: https://doi.org/10.1016/j.gca.2023.12.009.

Adams, B.A., Hodges, K.V., Whipple, K.X., Ehlers, T.A., van Soest, M.C., Wartho, J., 2015. Constraints on the tectonic and landscape evolution of the Bhutan Himalaya from thermochronometry. Tectonics 34, doi: https://doi.org/10.1002/2015TC003853.

Amundson, R., Heimsath, A., Jungers, M., Balan, S., Ebeling, A., Nishiizumi, K., Ewing, S., Shuster, D., Caffee, M.W., Pfeiffer, M., Dietrich, W.E., 2024. Relict soil evidence for post-Miocene aridification in the Atacama Desert of South America. Geological Society of America Bulletin 137, 465–480, doi: https://doi.org/10.1130/B37356.1.

Armijo, R., Lacassin, R., Coudurier-Curveur, A., Carrizo, D., 2015. Coupled tectonic evolution of Andean orogeny and global climate. Earth-Science Reviews 143, doi: https://doi.org/10.1016/j.earscirev.2015.01.005.

Avdievitch, N.N., Ehlers, T.A., Glotzbach, C., 2018. Slow long-term exhumation of the west central Andean plate boundary, Chile. Tectonics 37, 2243–2267, doi: https://doi.org/10.1029/2017TC004944.

Barnes, J.B., Ehlers, T.A., 2009. End member models for Andean Plateau uplift. Earth-Science Reviews 97, 105–132, doi: https://doi.org/10.1016/j.earscirev.2009.08.003.

Braun, J., 2003. Pecube: A new finite-element code to solve the 3D heat transport equation including the effects of a time-varying, finite amplitude surface topography. Computers & Geosciences 29, 787–794, doi: https://doi.org/10.1016/S0098-3004(03)00052-9.

Bufe, A., Rugenstein, J.K.C., Hovius, N., 2024. CO_2 drawdown from weathering is maximized at moderate erosion rates. Science 383, 1075–1080, doi: https://doi.org/10.1126/science.adk0957.

Burchardt, S., Tanner, D., Krumbholz, M., 2012. The Slaufrudalur pluton, southeast Iceland—An example of shallow magma emplacement by coupled cauldron subsidence and magmatic stoping. Geological Society of America Bulletin 124, 213–227, doi: https://doi.org/10.1130/B30430.1.

Carslaw, H.S., Jaeger, C.J., 1959. Conduction of Heat in Solids, 3rd Edition. Clarendon Press, Oxford, 510 pp.

Cernuschi, F., Dilles, J.H., Osorio, J., Proffett, J.M., Kouzmanov, K., 2023. A Reevaluation of the Timing and Temperature of Copper and Molybdenum Precipitation in Porphyry Deposits. Economic Geology 118, doi: https://doi.org/10.5382/econgeo.5032.

Charrier, R., Pinto, L., Rodríguez, M.P., 2007. Tectonostratigraphic evolution of the Andean Orogen in Chile. Moreno, T., Gibbons, W. (Eds.), Geological Society of London, doi: https://doi.org/10.1144/GOCH.

Chesley, J.T., Halliday, A.N., Snee, L.W., Mezger, K., Shepherd, T.J., Scrivener, R.C., 1993. Thermochronology of the Cornubian batholith in southwest England: Implications for pluton emplacement and protracted hydrothermal mineralization. Geochimica et Cosmochimica Acta 57, 1817–1835, doi: https://doi.org/10.1016/0016-7037(93)90115-D.

Coira, B., Davidson, J., Mpodozis, C., Ramos, V., 1982. Tectonic and magmatic evolution of the Andes of northern Argentina and Chile. Earth-Science Reviews 18, 303–332, doi: https://doi.org/10.1016/0012-8252(82)90042-3.

Cooper, F.J., Adams, B.A., Blundy, J.D., Farley, K.A., McKeon, R.E., Ruggiero, A.A., 2016. Aridity-induced Miocene canyon incision in the Central Andes. Geology 44, 675–678, doi: https://doi.org/10.1130/G38254.1.

Cruden, A.R., McCaffrey, K.J.W., Bunger, A.P., 2017. Geometric Scaling of Tabular Igneous Intrusions: Implications for Emplacement and Growth, in: Breitkreuz, C., Rocchi, S. (Eds.), Physical Geology of Shallow Magmatic Systems, Advances in Volcanology. Springer, Switzerland, doi: https://doi.org/10.1007/11157_2017_1000.

Dahlström, S.I.R., Cooper, F.J., Blundy, J., Tapster, S., Cortés Yáñez, J., Evenstar, L.A., 2022. Pluton Exhumation in the Precordillera of Northern Chile (17.8°–24.2°S):

Implications for the Formation, Enrichment, and Preservation of Porphyry Copper Deposits. Economic Geology 117, 1043–1071, doi: https://doi.org/10.5382/econgeo.4912.

Dilles, J.H., 1987. Petrology of the Yerington Batholith, Nevada: evidence for evolution of porphyry copper ore fluids. Economic Geology 82, 1750–1789, doi: https://doi.org/10.2113/gsecongeo.82.7.1750.

Ehlers, T.A., 2005. Crustal Thermal Processes and the Interpretation of Thermochronometer Data. Reviews in Mineralogy & Geochemistry 58, doi: ttps://doi.org/10.2138/rmg.2005.58.12.

Ehlers, T.A., 2023. Pecube-D: Thermokinematic and Erosion Modeling Software for problems in Tectonics and Surface Processes. Zenodo, doi: https://doi.org/10.5281/zenodo.7785668.

Evenstar, L.A., Dahlström, S.I.R., Hartley, A.J., McCuaig, T.C., Mather, A.E., Shaw, J.M., 2025. Global constraints on exhumation rates during porphyry copper formation and supergene enrichment: applications to exploration as illustrated from the Central Andes. Mineralium Deposita 60, 23–45, doi: https://doi.org/10.1007/s00126-024-01303-1.

Farley, K.A., 2000. Helium diffusion from apatite: General behavior as illustrated by Durango fluorapatite. Journal of Geophysical Research 105, 2903–2914, doi: https://doi.org/10.1029/1999JB900348.

Fox, M., Shuster, D.L., 2020. Lazed and Diffused: Untangling Noble Gas Thermochronometry Data for Exhumation Rates. Elements 16, 337–342, doi: https://doi.org/10.2138/gselements.16.5.337.

Furlong, K.P., Kirby, E., Creason, C.G., Kamp, P.J.J., Xu, G., Danišík, M., Shi, X., Hodges, K.V., 2021. Exploiting Thermochronology to Quantify Exhumation Histories and Patterns of Uplift Along the Margins of Tibet. Frontiers in Earth Science 9, doi: https://doi.org/10.3389/feart.2021.688374.

Galy, V., Peucker-Ehrenbrink, B., Eglinton, T., 2015. Global carbon export from the terrestrial biosphere controlled by erosion. Nature 521, 204–207, doi: https://doi.org/10.1038/nature14400.

Garzione, C.N., Hoke, G.D., Libarkin, J.C., Withers, S., MacFadden, B., Eiler, J., Ghosh, P., Mulch, A., 2008. Rise of the Andes. Science 320, 1304–1307, doi: https://doi.org/10.1126/science.1148615.

Glotzbach, C., van der Beek, P.A., Spiegel, C., 2011. Episodic exhumation and relief growth in the Mont Blanc massif, Western Alps from numerical modelling of thermochronology data. Earth and Planetary Science Letters 304, 417–430, doi: https://doi.org/10.1016/j.epsl.2011.02.020.

Haschke, M., Gunther, A., Melnick, D., Echtler, H., Reutter, H., Scheuber, K.-J., Oncken, O., 2006. Central and southern Andean tectonic evolution inferred from arc magmatism, in: Oncken, O., Chong, G., Franz, G., Giese, P., Götze, H.-J., Ramos, V., Strecker, M.R., Wigger, P. (Eds.), The Andes—Active Subduction Orogeny. Springer, Berlin, https://link.springer.com/chapter/10.1007/978-3-540-48684-8_16.

Hilton, R.G., West, A.J., 2020. Mountains, erosion and the carbon cycle. Nature Reviews Earth & Environment 1, 284–299, doi: https://doi.org/10.1038/s43017-020-0058-6.

Kober, F., Ivy-Ochs, S., Schlunegger, F., Baur, H., Kubik, P.W., Wieler, R., 2007. Denudation rates and a topography-driven rainfall threshold in northern Chile:

Multiple cosmogenic nuclide data and sediment yield budgets. Geomorphology 83, 97–120, doi: https://doi.org/10.1016/j.geomorph.2006.06.029.

Kober, F., Schlunegger, F., Zeilinger, G., Schneider, H., 2006. Surface uplift and climate change: The geomorphic evolution of the Western Escarpment of the Andes of northern Chile between the Miocene and present, in: Willett, S.D., Hovius, N., Brandon, M.T., Fisher, D.M. (Eds.), Tectonics, Climate, and Landscape Evolution. Geological Society of America Special Paper 398, doi: https://doi.org/10.1130/2006.2398(05).

Lee, C.-T., Thurner, S., Paterson, S., Cao, W., 2015. The rise and fall of continental arcs: Interplays between magmatism, uplift, weathering, and climate. Earth and Planetary Science Letters 425, 105–119, doi: https://doi.org/10.1016/j.epsl.2015.05.045.

Li, J., Qin, K., Li, G., Cao, M., Xiao, B., Chen, L., Zhao, J., Evans, N.J., McInnes, B.I.A., 2012. Petrogenesis and thermal history of the Yulong porphyry copper deposit, Eastern Tibet: insights from U-Pb and U-Th/He dating, and zircon Hf isotope and trace element analysis. Mineralogy and Petrology 105, 201–221, doi: https://doi.org/10.1007/s00710-012-0211-0.

Maksaev, V., Zentilli, M., 1999. Fission track thermochronology of the Domeyko Cordillera, northern Chile: Implications for Andean tectonics and porphyry copper metallogenesis. Exploration and Mining Geology 8, 65–89.

Martinod, J., Husson, L., Roperch, P., Guillaume, B., Espurt, N., 2010. Horizontal subduction zones, convergence velocity and the building of the Andes. Earth and Planetary Science Letters 299, 299–309, doi: https://doi.org/10.1016/j.epsl.2010.09.010.

Matzel, J.E.P., Bowring, S.A., Miller, R.B., 2006. Time scales of pluton construction at differing crustal levels: Examples from the Mount Stuart and Tenpeak intrusions, North Cascades, Washington. Geological Society of America Bulletin 118, 1412–1430, doi: https://doi.org/10.1130/B25923.1.

McCaffrey, K.J.W., Petford, N., 1997. Are granitic intrusions scale invariant? Journal of the Geological Society 154, 1–4, doi: https://doi.org/10.1144/gsjgs.154.1.0001.

McQuarrie, N., Horton, B.K., Zandt, G., Beck, S., DeCelles, P.G., 2005. Lithospheric evolution of the Andean fold-thrust belt, Bolivia, and the origin of the central Andean plateau. Tectonophysics 399, 15–37, doi: https://doi.org/10.1016/j.tecto.2004.12.013.

Michalak, M.J., Hall, S.R., Farber, D.L., Audin, L., Hourigan, J.K., 2016. (U-Th)/He thermochronology records late Miocene accelerated cooling in the north-central Peruvian Andes. Lithosphere 8, 103–115, doi: https://doi.org/10.1130/L485.1.

Michel, J., Baumgartner, L., Putlitz, B., Schaltegger, U., Ovtcharova, M., 2008. Incremental growth of the Patagonian Torres del Paine laccolith over 90 k.y. Geology 36, 459–462, doi: https://doi.org/10.1130/G24546A.1.

Mpodozis, C., Cornejo, P., 2012. Cenozoic Tectonics and Porphyry Copper Systems of the Chilean Andes. Society of Economic Geologists Special Publication 16, 329–360, doi: https://doi.org/10.5382/SP.16.14.

Muller, V.A.P., Sue, C., Valla, P.G., Sternai, P., Simon-Labric, T., Gautheron, C., Cuffey, K.M., Grujic, D., Bernet, M., Martinod, J., Ghiglione, M.C., Reiners, P., Willett, C., Shuster, D., Herman, F., Baumgartner, L., Braun, J., 2024. Geodynamic and Climatic Forcing on Late-Cenozoic Exhumation of the Southern Patagonian Andes (Fitz Roy and Torres del Paine massifs). Tectonics 43, doi: https://doi.org/10.1029/2023TC007914.

Murray, K.E., Braun, J., Reiners, P.W., 2018. Toward robust interpretation of low-temperature thermochronometers in magmatic terranes. Geochemistry, Geophysics, Geosystems 19, doi: https://doi.org/10.1029/2018GC007595.

Mutch, E.J.F., Blundy, J.D., Tattitch, B.C., Cooper, F.J., Brooker, R.A., 2016. An experimental study of amphibole stability in low-pressure granitic magmas and a revised Al-in-hornblende geobarometer. Contributions to Mineralogy and Petrology 171, doi: https://doi.org/10.1007/s00410-016-1298-9.

Nguyen, M.H., Carter, A., Hoang, L.V., Fox, M., Pham, S.N., Vinh, H.B., 2022. Evolution of the Continental Margin of South to Central Vietnam and Its Relationship to Opening of the South China Sea (East Vietnam Sea). Tectonics 41, doi: https://doi.org/10.1029/2021TC006971.

Pardo-Casas, F., Molnar, P., 1987. Relative motion of the Nazca (Farallon) and South American Plates since Late Cretaceous time. Tectonics 6, 233–248, doi: https://doi.org/10.1029/TC006i003p00233.

Perelló, J., 2003. Conchi porphyry copper deposit, Antofagasta region, northern Chile. Congreso Geológico Chileno, 10th, Concepción, Chile.

Pownall, J.M., Waters, D.J., Searle, M.P., Shail, R.K., Robb, L.J., 2012. Shallow laccolithic emplacement of the Land’s End and Tregonning granites, Cornwall, UK: Evidence from aureole field relations and P-T modeling of cordierite-anthophyllite hornfels. Geosphere 8, 1467–1504, doi: https://doi.org/10.1130/GES00802.1.

Rech, J.A., Currie, B.S., Jordan, T.H., Riquelme, R., Lehmann, S.B., Kirk-Lawlor, N.E., Li, S., Gooley, J.T., 2019. Massive middle Miocene gypsic paleosols in the Atacama Desert and the formation of the Central Andean rain-shadow. Earth and Planetary Science Letters 506, 184–194, doi: https://doi.org/10.1016/j.epsl.2018.10.040.

Reiners, P.W., Spell, T.L., Nicolescu, S., Zanetti, K.A., 2004. Zircon (U-Th)/He thermochronometry: He diffusion and comparisons with ^{40}Ar/^{39}Ar dating. Geochimica et Cosmochimica Acta 68, 1857–1887, doi: https://doi.org/10.1016/j.gca.2003.10.021.

Reiners, P.W., Thomson, S.N., Vernon, A., Willett, S.D., Zattin, M., Einhorn, J., Gehrels, G., Quade, J., Pearson, D., Murray, K.E., Cavazza, W., 2015. Low-temperature thermochronologic trends across the central Andes, 21°S–28°S, in: DeCelles, P.G., Ducea, M.N., Carrapa, B., Kapp, P.A. (Eds.), Geodynamics of a Cordilleran Orogenic System: The Central Andes of Argentina and Northern Chile, Geological Society of America Memoir 212, doi: https://doi.org/10.1130/9780813712123.

Ring, U., Brandon, M.T., Willett, S.D., Lister, G.S., 1999. Exhumation processes, in: Ring, U., Brandon, M.T., Lister, G.S., Willett, S.D. (Eds.), Exhumation Processes: Normal Faulting, Ductile Flow and Erosion. Geological Society, London Special Publications, doi: https://doi.org/10.1144/gsl.sp.1999.154.01.01.

Ruddiman, W.F., 1997. Tectonic Uplift and Climate Change. Ruddiman, W.F. (Ed.), Springer New York, doi: https://doi.org/10.1007/978-1-4615-5935-1.

Sanchez, C., Brichau, S., Riquelme, R., Carretier, S., Bissig, T., Lopez, C., Mpodozis, C., Campos, E., Regard, V., Hérail, G., Marquardt, C., 2018. Exhumation history and timing of supergene copper mineralisation in an arid climate: New thermochronological data from the Centinela District, Atacama, Chile. Terra Nova 30, 78–85, doi: https://doi.org/10.1111/ter.12311.

Schaltegger, U., Nowak, A., Ulianov, A., Fisher, C.M., Gerdes, A., Spikings, R., Whitehouse, M.J., Binderman, I., Hanchar, J.M., Duff, J., Vervoort, J.D., Sheldrake, T., Caricchi, L., Brack, P., Müntener, O., 2019. Zircon Petrochronology and ^{40}Ar/^{39}Ar Thermochronology of the Adamello Intrusive Suite, N. Italy: Monitoring the Growth and Decay of an Incrementally Assembled Magmatic System. Journal of Petrology 60, 701–722, doi: https://doi.org/10.1093/petrology/egz010.

Schildgen, T.F., Ehlers, T.A., Whipp, D.M., van Soest, M.C., Whipple, K.X., Hodges, K.V., 2009. Quantifying canyon incision and Andean Plateau surface uplift, southwest Peru: A thermochronometer and numerical modeling approach. Journal of Geophysical Research 114, doi: https://doi.org/10.1029/2009JF001305.

Schultz, M.H., Hodges, K.V., Ehlers, T.A., van Soest, M.C., Wartho, J.-A., 2017. Thermochronologic constraints on the slip history of the South Tibetan detachment system in the Everest region, southern Tibet. Earth and Planetary Science Letters 459, 105–117, doi: https://doi.org/10.1016/j.epsl.2016.11.022.

Sellés, D., Gardeweg, M., Garibaldi, N., 2016. Geología del área Pampa Lirima-Cancosa, Región de Tarapacá: Servicio Nacional de Geología y Minería, Carta Geológica de Chile, Serie Geología Básica, no. 182, scale 1:100,000.

Shaw, J.M., Evenstar, L.A., Cooper, F.J., Adams, B.A., Boyce, A.J., Hofmann, F., Farley, K.A., 2021. A Rusty Record of Weathering and Groundwater Movement in the Hyperarid Central Andes. G-Cubed 22, doi: https://doi.org/10.1029/2021GC009759.

Sillitoe, R.H., 2010. Porphyry Copper Systems. Economic Geology 105, 3–41, doi: https://doi.org/10.2113/gsecongeo.105.1.3.

Sillitoe, R.H., McKee, E.H., 1996. Age of supergene oxidation and enrichment in the Chilean porphyry copper province. Economic Geology 91, 164–179, doi: https://doi.org/10.2113/gsecongeo.91.1.164.

Stalder, N.F., Herman, F., Fellin, M.G., Coutand, I., Aguilar, G., Reiners, P.W., Fox, M., 2020. The relationships between tectonics, climate and exhumation in the Central Andes (18–36°S): Evidence from low-temperature thermochronology. Earth-Science Reviews 210, doi: https://doi.org/10.1016/j.earscirev.2020.103276.

Stüwe, K., White, L., Brown, R., 1994. The influence of eroding topography on steady-state isotherms. Application to fission track analysis. Earth and Planetary Science Letters 124, 63–74, doi: https://doi.org/10.1016/0012-821X(94)00068-9.

Thiede, R.C., Ehlers, T.A., 2013. Large spatial and temporal variations in Himalayan denudation. Earth and Planetary Science Letters 371–372, 278–293, doi: https://doi.org/10.1016/j.epsl.2013.03.004.

Tomlinson, A.J., Blanco, N., Maksaev, V., Dilles, J.H., Grunder, A.L., Ladino, M., 2001. Geología de la Precordillera Andina de Quebrada Blanca-Chuquicamata, Regiones I y II (20°30’S–22°30’S).

Valla, P.G., van der Beek, P.A., Shuster, D.L., Braun, J., Herman, F., Tassan-Got, L., Gautheron, C., 2012. Late Neogene exhumation and relief development of the Aar and Aiguilles Rouges massifs (Swiss Alps) from low-temperature thermochronology modeling and ^{4}He/^{3}He thermochronometry. Journal of Geophysical Research - Earth Surface 117, doi: https://doi.org/10.1029/2011JF002043.

van Soest, M.C., Monteleone, B.D., Hodges, K.V., Boyce, J.W., 2011. Laser depth profiling studies of helium diffusion in Durango fluorapatite. Geochimica et Cosmochimica Acta 75, 2409–2419, doi: https://doi.org/10.1016/j.gca.2011.02.008.

von Quadt, A., Erni, M., Martinek, K., Moll, M., Peytcheva, I., Heinrich, C.A., 2011. Zircon crystallization and the lifetimes of ore-forming magmatic-hydrothermal systems. Geology 39, 731–734, doi: https://doi.org/10.1130/G31966.1.

Weiland, R.J., Cloos, M., 1996. Pliocene-Pleistocene asymmetric unroofing of the Irian fold belt, Irian Jaya, Indonesia: Apatite fission-track thermochronology. Geological Society of America Bulletin 108, 1438–1449, doi: https://doi.org/10.1130/0016-7606(1996)108<1438:PPAUOT>2.3.CO;2.

Wilson, P.I.R., McCaffrey, K.J.W., Wilson, R.W., Jarvis, I., Holdsworth, R.E., 2016. Deformation structures associated with the Trachyte Mesa intrusion, Henry Mountains, Utah: Implications for sill and laccolith emplacement mechanisms. Journal of Structural Geology 87, 30–46, doi: https://doi.org/10.1016/j.jsg.2016.04.001.

Zhao, H., Wang, Q., Li, W., Shu, Q., Sun, X., Deng, J., 2022. The roles of emplacement depth, magma volume and local geologic conditions in the formation of the giant Yulong copper deposit, Eastern Tibet. Ore Geology Reviews 145, doi: https://doi.org/10.1016/j.oregeorev.2022.104877.